Crack-Like Sources of Dislocation Nucleation and Multiplication in Thin Films

D. E. Jesson; K. M. Chen; S. J. Pennycook; T. Thundat; R. J. Warmack

Science, New Series, Vol. 268, No. 5214 (May 26, 1995), 1161-1163.

Stable URL:
http://links.jstor.org/sici?sici=0036-8075%2819950526%293%3A268%3A5214%3C1161%3ACSODNA%3E2.0.CO%3B2-6

Science is currently published by American Association for the Advancement of Science.

Your use of the JSTOR archive indicates your acceptance of JSTOR's Terms and Conditions of Use, available at http://www.jstor.org/about/terms.html. JSTOR's Terms and Conditions of Use provides, in part, that unless you have obtained prior permission, you may not download an entire issue of a journal or multiple copies of articles, and you may use content in the JSTOR archive only for your personal, non-commercial use.

Please contact the publisher regarding any further use of this work. Publisher contact information may be obtained at http://www.jstor.org/journals/aaas.html.

Each copy of any part of a JSTOR transmission must contain the same copyright notice that appears on the screen or printed page of such transmission.

JSTOR is an independent not-for-profit organization dedicated to creating and preserving a digital archive of scholarly journals. For more information regarding JSTOR, please contact support@jstor.org.

http://www.jstor.org/
Fri Jun 4 15:06:10 2004

this approach is closely related to maximum likelihood methods of fitting models to data.
3. The number of bits required to specify the generative weights should also be included in the description length (*1*), but we currently ignore it.
4. G. E. Hinton and R. S. Zemel, in *Advances in Neural Information Processing Systems* J. D. Cowan, G. Tesauro, J. Alspector, Eds. (Kaufmann, San Mateo, CA, 1994), vol. 6, pp. 3–10.
5. An unbiased estimate of the exact gradient is easy to obtain, but the noise in this estimate increases with the size of the network. Alternatively, a mean-field approximation can be made to the stochastic recognition model and the error derivatives can then be computed by a back-propagation process (P. Dayan, G. E. Hinton, R. M. Neal, R. S. Zemel, *Neural Comput.*, in press).
6. This performs stochastic steepest descent in the Kullback-Leibler divergences

$$\sum_{i\in L}\sum_{j\in \ell} p_j^\gamma \log(p_j^\gamma/q_j^\gamma) + (1 - p_j^\gamma)\log[(1 - p_j^\gamma)/(1 - q_j^\gamma)] \quad (9)$$

The cost function in Eq. 5 contains the same terms but with p and q interchanged, leading to an approximation error that is equal to the asymmetry of the Kullback-Leibler divergences.
7. The training data was 700 examples of each digit from the CEDAR CDROM 1 made available by the U.S. Postal Service Office of Advanced Technology. Starting with the input layer, each of the 10 digit-specific networks had a 64-16-16-4 architecture. All weights were started at 0, and the learning rate on all connections was 0.01. Training involved 500 sweeps through the 700 examples. For testing, each net was run 10 times to estimate the expected description length of the image. The single network trained on all the digits had a 64-32-32-16 architecture and was also trained for 500 sweeps through the 7000 examples. If just the base rates of the individual pixels in the input were used, the average code length per test digit was 59.0 bits; if the 10 digit-specific networks were used, the average length was 33.8 bits, including the 3.3 bits required to specify which model was being used; if the single network was used, the average length was 37.3 bits.
8. In principal components analysis, the hidden representation vector is a linear function of the input vector and the aim is to minimize the squared reconstruction error. From a description length perspective, the cost of describing the hidden activities is ignored, so that only the cost of describing the reconstruction errors needs to be minimized. If these errors are coded with the use of a zero-mean Gaussian, the cost of describing them is proportional to their squared values. In competitive learning, only the hidden unit whose weight vector is most similar to the input vector is activated. The reconstruction is just the weight vector of the winning hidden unit, and so minimizing the squared distance between the input vector and the weight vector of the winning hidden unit minimizes the description length of the reconstruction error.
9. G. Carpenter and S. Grossberg, *Comput. Vision Graphics Image Process.* **37**, 54 (1987).
10. S. Ullman, in *Large-Scale Theories of the Cortex*, C. Koch and J. Davis, Eds. (MIT Press, Cambridge, MA, 1994), pp. 257–270.
11. M. Kawato, H. Hayakama, T. Inui, *Network: Comput. Neural Syst.* **4**, 415 (1993).
12. D. Mumford, in *Large-Scale Theories of the Cortex*, C. Koch and J. Davis, Eds. (MIT Press, Cambridge, MA, 1994), pp. 125–152.
13. M. I. Jordan and D. E. Rumelhart, *Cognitive Sci.* **16**, 307 (1992).
14. H. B. Barlow, *Neural Comput.* **1**, 295 (1989).
15. U. Grenander, *Lectures in Pattern Theory I, II, and III: Pattern Analysis, Pattern Synthesis, and Regular Structures*, (Springer-Verlag, Berlin, 1976–1981).
16. M. E. Hasselmo and J. M. Bower, *Trends Neurosci.* **16**, 218 (1993).
17. The learning rates were 0.2 for the generative and recognition weights to and from the input units and 0.001 for the other weights. The generative biases of the first hidden layer started at −3.00, and all other weights started at 0.0. The final asymmetric divergence between the network's generative model and the real data was 0.10 bit. The penalty term in Eq. 8 was 0.08 bit.
18. This research was supported by Canadian federal grants from the National Sciences and Engineering Research Council and the Institute for Robotic and Intelligent Systems and an Ontario grant from the Information Technology Research Centre. G.E.H. is the Noranda Fellow of the Canadian Institute for Advanced Research.

29 November 1994; accepted 4 April 1995

Crack-Like Sources of Dislocation Nucleation and Multiplication in Thin Films

D. E. Jesson,* K. M. Chen, S. J. Pennycook, T. Thundat, R. J. Warmack

With the combination of the height sensitivity of atomic force microscopy and the strain sensitivity of transmission electron microscopy, it is shown that near singular stress concentrations can develop naturally in strained epitaxial films. These crack-like instabilities are identified as the sources of dislocation nucleation and multiplication in films of high misfit. This link between morphological instability and dislocation nucleation provides a method for studying the basic micromechanisms that determine the strength and mechanical properties of materials.

Dislocation nucleation in thin films is of considerable scientific and technological importance in research areas ranging from the transport properties of superconducting layers to the regulation of electrical and optical properties in semiconductor devices. The mechanism by which the first dislocations nucleate in a continuous thin film has been a central and unresolved issue of strained-layer epitaxy. It is known that misfit stress in thin films can be relieved by the introduction of either a nonplanar surface morphology (*1–7*) or misfit dislocations (*8–10*), but the connection and relative importance of these mechanisms has not been explored. Furthermore, the identification of dislocation sources and multiplication mechanisms presents an outstanding experimental challenge.

Here we study strain relaxation in the technologically important Si-Ge system, which illustrates the general physical principles governing the growth of strained thin films. Our approach is to combine atomic force microscopy (AFM) with transmission electron microscopy (TEM) to provide complementary local height and strain information. This procedure reveals that crack-like surface instabilities develop spontaneously and act as the sources of misfit dislocations in strained thin films. These observations connect the previously disparate fields of morphological instability and dislocation nucleation through the natural framework of fracture mechanics.

To examine the connection between dislocation nucleation and morphological instability at high misfits, it is necessary to study the critical transition regime between a coherent (highly stressed) and dislocated (partially relaxed) film. This transition, which occupies only a very small region of the enormous phase space of deposition variables, was achieved in two stages. Initially, a 10-nm-thick $Si_{0.5}Ge_{0.5}$ alloy layer was deposited on Si(001) by molecular beam epitaxy at 400°C to create a dislocation-free film associated with a nominally planar surface. The morphological instability of this surface was demonstrated by a 1-min in situ anneal at 560°C, during which a surface ripple morphology develops, as shown in Fig. 1, A and B. The ripple consists of island-like features that align along the elastically soft [100] and [010] directions, resulting in an arrangement of orthogonal domains. Typically, the islands are 15 nm high and 100 nm in diameter, with a strong tendency to facet along {501} planes. The formation of these low-energy planes would seem to stabilize the misfit-induced morphological instability, resulting in a network of significantly stressed valleys at island intersections located ~4 nm above the alloy-substrate interface. We would emphasize that this situation results from the instability of a planar film surface and is appreciably different from the case in which the film grows initially by means of isolated islands (*11*) or fractures to create islands (*12*).

The AFM image in Fig. 1A directly links this critical point in morphological instability with the onset of dislocation nucleation (*13*). Although island heights range from 13 to 18 nm, the dislocations (arrowed) are always associated with the tallest islands.

D. E. Jesson, K. M. Chen, S. J. Pennycook, Solid State Division, Oak Ridge National Laboratory, Oak Ridge, TN 37831, USA.
T. Thundat and R. J. Warmack, Health Sciences Research Division, Oak Ridge National Laboratory, Oak Ridge, TN 37831, USA.
*To whom correspondence should be addressed.

The dislocation density is 10^7 cm^{-2}, which is three orders of magnitude greater than the threading dislocation density in the substrate. Thus, the height sensitivity of AFM demonstrates that a surprisingly small amount of surface ripple is sufficient to induce dislocation nucleation. A Burgers vector analysis by weak beam TEM (Fig. 2B) reveals that the dislocations are, surprisingly, of the perfect 90° edge type. After nucleation, they can be seen to propagate in ⟨110⟩ directions parallel to the alloy-substrate interface. The most likely propagation mechanism of sessile 90° dislocations is by the decomposition of one end of the dislocation into two 60° threading segments, which then propagate parallel to the 90° dislocation line on {111} planes. Each dislocated island is relaxed by ~0.4% in a direction perpendicular to the dislocation line. The subsequent alignment of adjacent islands presents a clear fingerprint of dislocation passage, allowing the height sensitivity of AFM to provide unique insight into the relaxation processes.

The detailed nature of the dislocation source and mechanism of nucleation is revealed by plan view TEM (Fig. 2, A and B) (*14*). Although the regions between dislocation-free islands are under appreciable compressive stress, remarkably sharp stress concentration lines (S) occasionally occur along ⟨110⟩ directions. From the narrow width and magnitude of the weak beam images, we can deduce that the stress lines are manifestations of the crack-like surface instabilities considered theoretically by Yang and Srolovitz (*15*) and observed in cross section by Jesson *et al.* (*16*). The critical stress concentrations responsible for dislocation nucleation are at 45° to the prominent ⟨100⟩ surface ripple. Presumably, the strong tendency for the surface to facet along {501} planes kinetically stabilizes the ripple morphology along elastically soft ⟨100⟩ directions, preventing the formation of deep cracks. Therefore, ⟨110⟩ crack-like stabilities arise at intersections between islands belonging to different ⟨100⟩ domains. This avoids the low-energy {501} planes so that the stress concentration is free to evolve (*15, 16*). The strain field of the cusp-like intersection under compression is formally the reverse of a crack under tension (*17*), which is consistent with the nature of our weak beam images (Fig. 2B). We therefore propose a crack blunting mechanism as a general method of dislocation injection during strained-layer epitaxy, as shown schematically in Fig. 3. To blunt the crack tip and nucleate a dislocation, it is only necessary to shear a single crystal plane. The dislocation, if sessile, is then "trapped" by the motion of the film surface during the growth or anneal.

According to a dislocation emission analysis based on the Peierls concept, the critical island height d^{φ} for nucleation is given by (*18*)

$$d^{\varphi} = \frac{16\mu\gamma_{us}^{\varphi}[1 + (1 - \nu)\cot^2\varphi]}{\pi\sigma^2(1 - \nu)(1 + \cos\theta)\sin^2\theta} \quad (1)$$

Here, θ is the angle between the glide and fracture plane, φ is the angle between the Burgers vector and the dislocation line, μ is the shear modulus, ν is Poisson's ratio, and σ is the misfit stress. The unstable stacking energy γ_{us}^{φ} is defined by Rice (*18*) and characterizes the resistance to dislocation nucleation. The competition between γ_{us}^{φ} and the dislocation geometry embodied in Eq. 1 is central to the physics of crack blunting and the brittle-to-ductile transition.

Our surprising observation that 90° dislocations nucleate in preference to other dislocation types at crack-like instabilities provides important information on the role of these quantities. The nucleation of a complete 60° dislocation or dissociated partials is likely to involve first the nucleation of a 30° partial on a (111) glide plane. As the in-plane shear stress is greater on the 30° (111) glide plane than on the 90° (001) glide plane, this will favor nucleation of the 30° partial. However, the pure edge nature of the 90° dislocation more than compensates for this reduction and so it experiences the greater force. Our experimental observation of 90° edge dislocations establishes

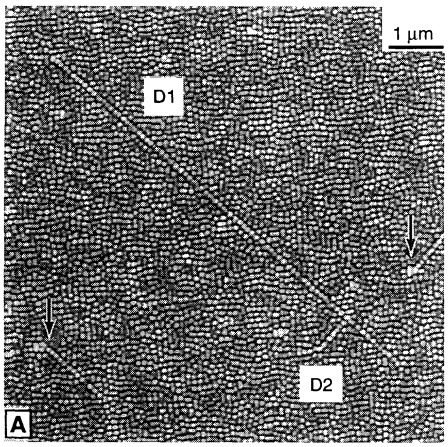

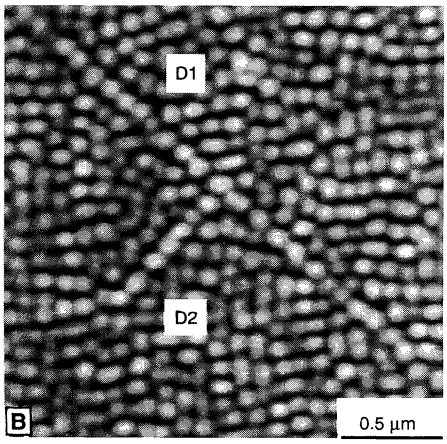

Fig. 1. (**A**) AFM image that shows dislocation nucleation as a result of the morphological instability of a $Si_{0.5}Ge_{0.5}$ alloy film. The dislocations (arrowed) are associated with the tallest "islands" corresponding to the brightest regions of the gray scale. (**B**) An expanded view of the junction between D1 and D2 where the primary dislocation D1 acts as a source for the secondary dislocation D2. The tendency of the islands to align along [100] (vertical) and [010] (horizontal) directions results in a domain-like surface ripple.

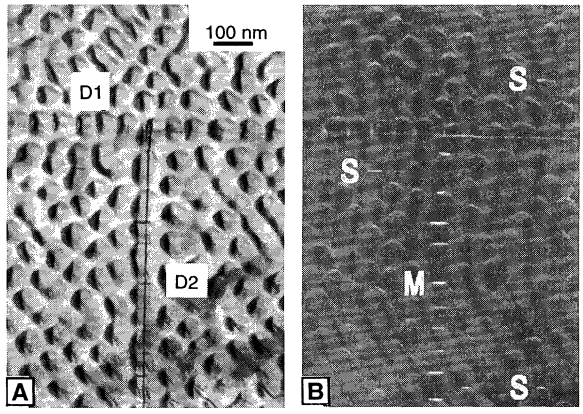

Fig. 2. (**A**) Bright-field (220) two-beam and (**B**) (2$\bar{2}$0) (*g*, 3*g*) weak beam TEM images of dislocation multiplication induced by morphological instability. High stress concentrations associated with the crack-like instabilities (S and M) are revealed as short bright segments in (B). The dislocation lines D1 and D2 define [110] and [1$\bar{1}$0] directions, respectively. The nature of the diffraction conditions means that dislocation D2 is in strong contrast in (A), and D1 is in contrast in (B). Similarly, stress lines (M) associated with D2 are in strong contrast in (B).

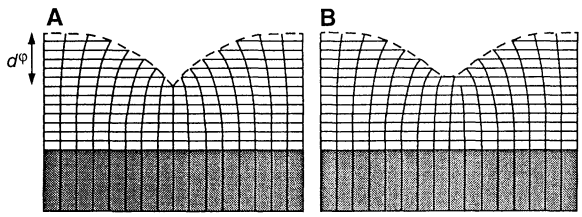

Fig. 3. The crack blunting mechanism of dislocation nucleation proposed for thin-film relaxation. The stress concentration at the tip of the crack-like instability shown in (**A**) results in the development of a 90° dislocation (**B**). This dislocation blunts the tip and lowers the stress concentration by analogy with a crack under tension.

that $d^{60} > d^{90}$, so that from Eq. 1 $\gamma_{us}^{90}/\gamma_{us}^{30} < 5.3$. Recent ab initio calculations of γ_{us}^{30} (*19*) then imply $\gamma_{us}^{90} < 8.85$ J m^{-2}. In the nonuniform field at the crack-like tip, the perfect edge character of the 90° dislocations would, therefore, appear to dominate the nucleation process, explaining why 90° dislocations are nucleated in preference to 60° dislocations (*20*).

A most surprising feature of Fig. 1 is the secondary dislocation (D2) that arises from the primary dislocation line (D1). We have observed a large number of isolated dislocation junctions consisting of short but multiply branched segments; this observation has led us to the conclusion that an existing dislocation can act as a multiplication source. This idea can also be understood in terms of our crack blunting nucleation mechanism. The partially relaxed islands decorating D1 provide low-energy binding sites for diffusing adatoms and grow preferentially during the annealing process. However, the 90° edge dislocation cannot relieve the stress along the direction of the dislocation line, and this stress will continue to increase as the islands grow in size. This stress is clearly a maximum at the island intersections orthogonal to the dislocation line, as evidenced by the distribution of stress lines (M) visible by weak beam TEM in Fig. 2B. It is therefore valid to consider multiplication as an efficient exploitation of primary nucleation because an existing dislocation line provides a large density of highly stressed island intersections. In order to relieve the stress concentration, D2 must be orthogonal to D1 as observed in Figs. 1 and 2.

The nucleation of 90° dislocations in high-misfit films has been a subject of some controversy because these dislocations are unable to glide to the interface. Various formation mechanisms have been proposed that involve the reaction of 60° dislocations (*21*, *22*). Although it is conceivable that such mechanisms may occur, our observations have revealed a direct nucleation path for 90° dislocations driven by stress concentrations at crack-like instabilities. Furthermore, this mechanism suggests the possibility of the opposite process in thicker films: A 90° dislocation that nucleates away from the interface in the residual strain field of the tip may subsequently decompose into two 60° dislocations, which glide to the interface on different (111) planes under the action of the misfit stress. This will be an activated process requiring a sufficiently thick wetting layer for the decomposition to occur, which explains the stability of the 90° dislocations in our images. Under these circumstances, the critical thickness for dislocation nucleation will depend on the formation kinetics of the crack-like instability geometry defined by Eq. 1.

Dislocation emission at crack-like surface instabilities that develop naturally during the growth of high misfit films can provide insights into the basic physics of subcritical crack growth and crack blunting in a controlled and clean environment. An accurate characterization of the unstable tip geometry based on surface microscopies and a comparison with thermally activated models of dislocation emission should allow the extraction of core parameters or unstable stacking energies. This may lead to advances in our understanding of the brittle-to-ductile transition and to a determination of the chief causes of the fracture and failure of materials in service.

REFERENCES AND NOTES

1. R. J. Asaro and W. A. Tiller, *Metall. Trans.* **3**, 1789 (1972).
2. M. A. Grinfeld, *Sov. Phys. Dokl.* **31**, 831 (1986).
3. D. J. Srolovitz, *Acta Metall.* **37**, 621 (1989).
4. A. J. Pidduck, D. J. Robbins, A. G. Cullis, W. Y. Leong, A. M. Pitt, *Thin Solid Films* **222**, 78 (1992).
5. D. J. Eaglesham and M. Cerullo, *Phys. Rev. Lett.* **64**, 1943 (1990).
6. B. J. Spencer, P. W. Voorhees, S. H. Davies, *J. Appl. Phys.* **73**, 4955 (1993).
7. C. W. Snyder, B. G. Orr, D. Kessler, L. M. Sander, *Phys. Rev. Lett.* **66**, 3032 (1991).
8. J. H. van der Merwe, *J. Appl. Phys.* **34**, 123 (1963).
9. S. V. Kamat and J. P. Hirth, *ibid.* **67**, 6844 (1990).
10. L. B. Freund, *Mater. Res. Soc. Res. Bull.* **17**, 52 (1992).
11. R. Vincent, *Philos. Mag.* **19**, 1127 (1969).
12. J. W. Matthews, *ibid.* **23**, 1405 (1971).
13. AFM images were acquired in the tapping mode (Digital Instruments, Santa Barbara, CA) in a dry, He-filled glove box.
14. TEM was performed on a Philips EM400 microscope operated at 100 keV.
15. W. H. Yang and D. J. Srolovitz, *Phys. Rev. Lett.* **71**, 1593 (1993).
16. D. E. Jesson, S. J. Pennycook, J.-M. Baribeau, D. C. Houghton, *ibid.*, p. 1744.
17. C-H. Chiu and H. Gao, *Int. J. Solids Struct.* **30**, 2983 (1993).
18. J. R. Rice, *J. Mech. Phys. Solids* **40**, 239 (1992).
19. E. Kaxiras and M. S. Duesbery, *Phys. Rev. Lett.* **70**, 3752 (1993).
20. An alternative nucleation mechanism involving the coalescence of two faces of a cusp to trap a hollow dislocation core has been proposed by J. Grilhé [*Europhys. Lett.* **23**, 141 (1993)]. However, it seems likely that in many systems the criteria for crack blunting will be met first before coalescence can occur.
21. J. S. Ahearn and C. Laird, *J. Mater. Sci.* **12**, 699 (1977).
22. S. A. Dregia and J. P. Hirth, *J. Appl. Phys.* **69**, 2169 (1991).

23. We acknowledge helpful discussions with G. E. Beltz. We thank M. F. Chisholm for comments on the manuscript, and we are grateful to A. J. McGibbon for assistance with the figures. This research was sponsored by the Division of Materials Sciences, U.S. Department of Energy, under contract DE-AC05-84OR21400 with Martin Marietta Energy Systems, Inc.

18 November 1994; accepted 24 February 1995

Efficient Oxidative Dechlorination and Aromatic Ring Cleavage of Chlorinated Phenols Catalyzed by Iron Sulfophthalocyanine

Alexander Sorokin, Jean-Louis Séris, Bernard Meunier*

An efficient method has been developed for the catalytic oxidation of pollutants that are not easily degraded. The products of the hydrogen peroxide (H_2O_2) oxidation of 2,4,6-trichlorophenol (TCP) catalyzed by the iron complex 2,9,16,23-tetrasulfophthalocyanine (FePcS) were observed to be chloromaleic, chlorofumaric, maleic, and fumaric acids from dechlorination and aromatic cycle cleavage, as well as additional products that resulted from oxidative coupling. Quantitative analysis of the TCP oxidation reaction revealed that up to two chloride ions were released per TCP molecule. This chemical system, consisting of an environmentally safe oxidant (H_2O_2) and an easily accessible catalyst (FePcS), can perform several key steps in the oxidative mineralization of TCP, a paradigm of recalcitrant pollutants.

Halogenated aromatic compounds are common environmental pollutants because of their halogen content (*1*). Many of these pollutants can be converted into less dangerous organic products and can be eventually degraded by different microorganisms (*1–3*). However, some of these chlorinated compounds are extremely persistent in the environment because of their slow degradation by reductive or oxidative enzymatic pathways (*4*, *5*). Systems that can remove halogen substituents from aromatics may produce compounds that can be more easily biodegraded. Efficient chemical catalysts are needed that can oxidatively degrade halogenated phenols, especially industrial effluents that include large amounts of chemicals that can overload the transformation capacity of microorganisms. In this case, the use of chemical catalysts to convert recalcitrant pollut-

A. Sorokin and B. Meunier, Laboratoire de Chimie de Coordination du CNRS, 205 route de Narbonne, 31077 Toulouse Cedex, France.
J.-L. Séris, Elf-Aquitaine, GRL-Biotechnology, Lacq, 64170 Artix, France.

*To whom correspondence should be addressed.